Structural Engineering and Mechanics, *Vol. 74, No. 2 (2020) 297-311*
DOI: https://doi.org/10.12989/sem.2020.74.2.297

Mechanical analysis of functionally graded spherical panel resting on elastic foundation under external pressure

Yan Cao*[1], Xueming Qian[1], Qingming Fan[1] and Farbod Ebrahimi**[2]

[1]*School of Mechatronic Engineering and Shaanxi Key Laboratory of Non-Traditional Machining, Xi'an Technological University, Xi'an 710021 China*
[2]*Young Researchers and Elite Club, Tehran Branch, Islamic Azad University, Tehran, Iran*

(Received June 7, 2019, Revised January 27, 2020, Accepted February 10, 2020)

Abstract. The main purpose of this study is to analyze the effects of external pressure on the vibration and buckling of functionally graded (FG) spherical panels resting of elastic medium. The material characteristics of the FG sphere continuously vary through the thickness direction based on the power-law rule. In accordance with first-order shear deformation shell theory and by the use of Ritz formulation the governing equations are presented. In this regard, the beam functions are applied in two-dimensions for different sets of boundary supports. The Winkler and Pasternak models of elastic foundations are also taken into account. In order to show the validity and applicability of the presented formulation, various comparison studies are given. Furthermore, a diverse range of numerical results is reported to check the impacts of geometrical and material parameters along with external pressure on the vibration and buckling analysis of FG spherical panels.

Keywords: functionally graded materials; spherical panel; vibration; buckling; beam functions

1. Introduction

Due to the desired performance in dynamic behavior and stability, thin and thick shells and panels have been extensively used in many different engineering applications such as aerospace structures and civil constructions. Meanwhile, owing to specific geometric shapes, the spherical shells and panels are used in various engineering applications. On the other hand, functionally graded (FG) materials are introduced as the novel composites in which the material properties change in a smooth way from one surface to another in a specific direction. By increasing the employment of FG spherical shells, the complete understanding of mechanical characteristics of these structures has a significant effect on engineers for proper design.

In last two decades, a wide range of research works have been performed on the vibration and buckling analysis of FG (Loy *et al*. 1999, Kar and Panda 2015, Patel *et al*. 2005, Tornabene 2009, Karroubi and Irani-Rahaghi 2019, Ghannad *et al*. 2012, Su *et al*. 2014, Alijani *et al*. 2011, Foroutan *et al*. 2018, Sofiyev *et al*. 2016, Bich *et al*. 2013) and functionally graded carbon nanotube reinforced composite (FG-CNTRC) (Heydarpour *et al*. 2014, Ansari and Torabi 2016, Shen and Xiang 2012, Torabi and Ansari 2018, Thomas and Roy 2016) shell structures. For instance, vibration analysis of FG elliptical cylindrical shells was presented by Patel *et al*. (2005) based on higher-order shell theory. Tornabene (2009) and Su *et al*. (2014) investigated the free vibration of FG conical/cylindrical shells based on first-order shear deformation theory (FSDT). The nonlinear vibration analysis of FG doubly-curved shallow shells was presented by Alijani *et al*. (2011) on the basis of Donnell's shell theory. Galerkin method along with multiple scales method was employed to find the nonlinear frequency responses. Ansari and Torabi (2016) highlighted the buckling and vibration analysis of FG-CNTRC conical shells using the numerical approach.

On the other hand, different numerical approaches such as generalized/harmonic differential quadrature method (Striz *et al*. 1997, Civalek and Ülker 2004, Hasrati *et al*. 18, Wu *et al*. 2018,), discrete convolution method (Civalek 2006, Civalek and Akar 2007, Civalek 2007, Civalek 2008, Akgoz and Civalek 2011, Mercan *et al*. 2016), finite element method (Song *et al*. 2006, Jung *et al*. 2016, Darilmaz 2017, Torabi and Ansari 2018) and finite strip method (Foroughi and Azhari 2014, Naghsh *et al*. 2015, Khayat *et al* 2016) have been employed to study the vibration and buckling of solid structures. For instance, the harmonic differential quadrature method was employed by Civalek and Ülker (2004) to analyze the axisymmetric bending analysis of thin isotropic circular plates. Civalek (2006, 2007, 2008) performed various studies on the vibration analysis of cylindrical and conical shells using the discrete convolution method. Naghsh *et al*. (2015) also used the finite strip method to study the free vibration of stringer stiffened general shells of revolution.

In comparison to other types of shell structures, fewer studies have been focused on the structural analysis of FG spherical shells and panels. Ganapati (2007) analyzed the dynamic stability behavior of FG shallow spheres subjected

*Corresponding author, Ph.D.
E-mail: jantonyz@163.com
**Co-corresponding author, Ph.D.
E-mail: fbd.ebrahimi@gmail.com

ISSN: 1225-4568 (Print), 1598-6217 (Online)

to external pressure. Newmark's integration scheme along with the modified Newton–Raphson technique was employed to solve the nonlinear governing equations. Shahsiah *et al*. (2006) investigated the thermal buckling FG shallow spherical shells. The analytical large-amplitude axisymmetric analysis (2011) and buckling analysis (2013) of FG shallow spheres subjected to pressure was highlighted by Bich and his co-authors. The temperature dependency of the material properties was taken into account. By considering initial imperfection and geometric non-linearity, the governing equations were derived using the classical shell theory. The nonlinear dynamics of FG spherical shells under low-velocity impact was reported by Mao *et al*. 2011. The thermal environment with steady-state heat conditions was also considered. Xie *et al*. (2015) studied the vibration of four-parameter FG spherical and parabolic circular shells with different boundary supports. The governing equations were derived in accordance with FSDT and the Haar Wavelet Discretization technique was employed to solve the problem. Wang *et al*. (2018) and Ansari *et al*. (2016) presented different studies on the vibration analysis of FG-CNTRC spherical shells An FSDT. In addition, by the use of a modified Fourier series-based Rayleigh-Ritz method, the 3D vibration of laminated FG spheres with general supports was investigated by Ye *et al*. (2014). Furthermore, the unified analytical solution procedure was introduced by Su *et al*. (2014 b,c) for free vibration analysis of FG panels.

Although, various investigations have been carried out on the vibration analysis of FG spherical shells, however, the effects of thermo-mechanical loadings on the vibrational characteristics were less considered. In this regard, the dynamic and stability analysis of FG spherical panels resting on elastic medium under external pressure is presented in this study. In other words, Studying the effects of the elastic foundation and external pressure on the vibration and buckling analyses of FG spherical panels is the main novel aspect of this research study. The continuous variation of the material properties along the thickness direction is considered for FG materials. In order to model the elastic medium, the Winkler and Pasternak models are considered. The basic equations of the structure are given on the basis of the FSDT. The Ritz formation based on the two-dimensional beam functions is employed for different sets of boundary conditions to obtain the governing equations. In addition to different comparative studies, a wide range of numerical results are expressed to examine the effects of involved factors on the vibration and buckling of FG spherical panels.

2. Governing equations

FG spherical panel with radius R and thickness h is considered. The geometry of the panel is defined in accordance with the spherical coordinate system of φ, θ and z along the meridional, circumferential and radial directions, as shown in Fig. 1. The overall material properties of FG panel smoothly vary through the thickness direction on the basis of the power-law as follows

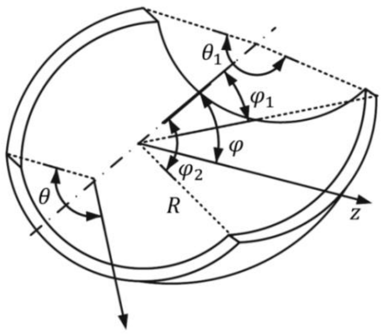

Fig. 1 Geometry and coordinate system of spherical panel

$$P(z) = P_m + P_{cm}\left(\frac{1}{2}+\frac{z}{h}\right)^k \quad , \quad P_{cm} = P_c - P_m \tag{1}$$

in which P_m and P_c stand for the material properties related to material and ceramic phases, respectively. In addition, volume fraction index $k\ (k \geq 0)$ denotes the material distribution profile. On the basis of the FSDT, the displacement components are expressed as

$$\begin{aligned} u_1 &= u_0 + z\,\psi_0(\varphi,\theta,t),\\ u_2 &= v_0 + z\,\phi_0(\varphi,\theta,t),\\ u_3 &= w_0(\varphi,\theta,t) \end{aligned} \tag{2}$$

where u_0, v_0 and w_0 are the displacement of mid-plane and ψ_0 and ϕ_0 stand for the rotations. The strain-displacement relations are given as

$$\begin{Bmatrix}\epsilon_{\varphi\varphi}\\ \epsilon_{\theta\theta}\\ \gamma_{\varphi\theta}\\ \gamma_{\theta z}\\ \gamma_{\varphi z}\end{Bmatrix} = \begin{Bmatrix}\epsilon^0_{\varphi\varphi}\\ \epsilon^0_{\theta\theta}\\ \gamma^0_{\varphi\theta}\\ \gamma^0_{\theta z}\\ \gamma^0_{\varphi z}\end{Bmatrix} + z\begin{Bmatrix}\chi_{\varphi\varphi}\\ \chi_{\theta\theta}\\ \chi_{\varphi\theta}\\ 0\\ 0\end{Bmatrix}, \tag{3}$$

with

$$\begin{aligned}
\epsilon^0_{\varphi\varphi} &= \frac{1}{R}\frac{\partial u_0}{\partial\varphi}, \qquad \chi_{\varphi\varphi} = \frac{1}{R}\frac{\partial\psi_0}{\partial\varphi},\\
\epsilon^0_{\theta\theta} &= \frac{1}{R_1}\frac{\partial v_0}{\partial\theta} + \frac{u_0\cos(\varphi)}{R_1} + \frac{w_0}{R},\\
\chi_{\theta\theta} &= \left(\frac{\psi_0\cos(\varphi)}{R_1} + \frac{1}{R_1}\frac{\partial\phi_0}{\partial\theta}\right),\\
\gamma^0_{\varphi\theta} &= \frac{1}{R_1}\frac{\partial u_0}{\partial\theta} + \frac{1}{R}\frac{\partial v_0}{\partial\varphi} - \frac{v_0\cos(\varphi)}{R_1},\\
\chi_{\varphi\theta} &= \left(\frac{1}{R_1}\frac{\partial\psi_0}{\partial\theta} + \frac{1}{R}\frac{\partial\phi_0}{\partial\varphi} - \frac{\phi_0\cos(\varphi)}{R_1}\right),\\
\gamma^0_{\theta z} &= \frac{1}{R_1}\frac{\partial w_0}{\partial\theta} - \frac{v_0}{R} + \phi_0, \qquad \gamma^0_{\varphi z} = \frac{1}{R}\frac{\partial w_0}{\partial\varphi} - \frac{u_0}{R} + \psi_0
\end{aligned} \tag{4}$$

in which $R_1 = R\sin(\varphi)$. In addition, the stress vector is presented in accordance with the following constitutive equation

$$\begin{Bmatrix}\sigma_{\varphi\varphi}\\ \sigma_{\theta\theta}\\ \tau_{\varphi\theta}\\ \tau_{\theta z}\\ \tau_{\varphi z}\end{Bmatrix} = \begin{bmatrix} Q_{11} & Q_{12} & 0 & 0 & 0\\ Q_{12} & Q_{11} & 0 & 0 & 0\\ 0 & 0 & Q_{66} & 0 & 0\\ 0 & 0 & 0 & Q_{66} & 0\\ 0 & 0 & 0 & 0 & Q_{66}\end{bmatrix}\begin{Bmatrix}\epsilon_{\varphi\varphi}\\ \epsilon_{\theta\theta}\\ \gamma_{\varphi\theta}\\ \gamma_{\theta z}\\ \gamma_{\varphi z}\end{Bmatrix} \tag{5}$$

with

$$Q_{11} = \frac{E(z)}{1+\nu(z)^2},\quad Q_{12} = \frac{\nu(z)E(z)}{1+\nu(z)^2},\ Q_{66} = \frac{E(z)}{2(1+\nu(z))} \tag{6}$$

where $E(z)$ and $\nu(z)$ are Young's modulus and Poisson's ratio, respectively. Based on the integration of stress field along the thickness direction, the force and moment resultants are obtained as

$$\begin{Bmatrix} N_{\varphi\varphi} \\ N_{\theta\theta} \\ N_{\varphi\theta} \\ M_{\varphi\varphi} \\ M_{\theta\theta} \\ M_{\varphi\theta} \\ Q_{\theta z} \\ Q_{\varphi z} \end{Bmatrix} = \begin{bmatrix} A_{11} & A_{12} & 0 & B_{11} & B_{12} & 0 & 0 & 0 \\ A_{12} & A_{11} & 0 & B_{12} & B_{11} & 0 & 0 & 0 \\ 0 & 0 & A_{66} & 0 & 0 & B_{66} & 0 & 0 \\ B_{11} & B_{12} & 0 & D_{11} & D_{12} & 0 & 0 & 0 \\ B_{12} & B_{11} & 0 & D_{12} & D_{11} & 0 & 0 & 0 \\ 0 & 0 & B_{66} & 0 & 0 & D_{66} & 0 & 0 \\ 0 & 0 & 0 & 0 & 0 & 0 & \kappa A_{44} & 0 \\ 0 & 0 & 0 & 0 & 0 & 0 & 0 & \kappa A_{55} \end{bmatrix} \begin{Bmatrix} \varepsilon^0_{\varphi\varphi} \\ \varepsilon^0_{\theta\theta} \\ \gamma^0_{\varphi\theta} \\ \chi_{\varphi\varphi} \\ \chi_{\theta\theta} \\ \chi_{\varphi\theta} \\ \gamma_{\theta z} \\ \gamma_{\varphi z} \end{Bmatrix} \tag{7}$$

where κ is the shear correction factor and A_{ij}, B_{ij} and D_{ij} are defined as

$$A_{ij} = \int_{-\frac{h}{2}}^{\frac{h}{2}} Q_{ij}\, dz, \qquad B_{ij} = \int_{-\frac{h}{2}}^{\frac{h}{2}} Q_{ij} z\, dz, \qquad D_{ij} = \int_{-\frac{h}{2}}^{\frac{h}{2}} Q_{ij}\, z^2 dz, \qquad (ij = 11,12,66) \tag{8}$$

Now, the elastic strain energy of the FG spherical panel can be defined as

$$U = \frac{1}{2}\int_A \int_{-h/2}^{h/2} (\sigma_{\varphi\varphi}\varepsilon_{\varphi\varphi} + \sigma_{\theta\theta}\varepsilon_{\theta} + \sigma_{\varphi\theta}\gamma_{\varphi\theta} + \sigma_{\varphi z}\gamma_{\varphi z} + \sigma_{\theta z}\gamma_{\theta z})\, dzdA \tag{9}$$

Furthermore, the kinetic energy is presented according to the following expression

$$T = \frac{1}{2}\int_{-\frac{h}{2}}^{\frac{h}{2}}\int_A \rho(z)\left[\left(\frac{\partial u_1}{\partial t}\right)^2 + \left(\frac{\partial u_2}{\partial t}\right)^2 + \left(\frac{\partial u_3}{\partial t}\right)^2\right] dAdz \tag{10}$$

which can be rewritten as

$$T = \frac{1}{2}\int_A \left\{ J_0\left[\left(\frac{\partial u_0}{\partial t}\right)^2 + \left(\frac{\partial v_0}{\partial t}\right)^2 + \left(\frac{\partial w_0}{\partial t}\right)^2\right] + J_1\left[\frac{\partial u_0}{\partial t}\frac{\partial \psi_0}{\partial t} + \frac{\partial v_0}{\partial t}\frac{\partial \phi_0}{\partial t}\right] + J_2\left[\left(\frac{\partial \psi_0}{\partial t}\right)^2 + \left(\frac{\partial \phi_0}{\partial t}\right)^2\right]\right\} dA \tag{11}$$

with

$$(J_0, J_1, J_2) = \int_{-\frac{h}{2}}^{\frac{h}{2}} \rho(z)(1, z, z^2) dz \tag{12}$$

Additionally, the potential energy of the elastic foundation is

$$U_f = \frac{1}{2}\int_A \left\{ K_w w_0^2 + K_g \left[\left(\frac{1}{R}\frac{\partial w_0}{\partial \varphi}\right)^2 + \left(\frac{1}{R_1}\frac{\partial w_0}{\partial \theta}\right)^2\right]\right\} dA \tag{13}$$

where K_w and K_g are Winkler and Pasternak coefficients of the elastic medium. Finally, the potential energy due to external force can be expressed as

$$U_e = \frac{1}{2}\int_A \left\{\left[N^0_{\varphi\varphi}\left(\frac{1}{R}\frac{\partial w_0}{\partial \varphi}\right)^2 + N^0_{\theta\theta}\left(\frac{1}{R_1}\frac{\partial w_0}{\partial \theta}\right)^2 + N^0_{\varphi\theta}\left(\frac{1}{RR_1}\frac{\partial w_0}{\partial \varphi}\frac{\partial w_0}{\partial \theta}\right)\right]\right\} dA \tag{14}$$

where N^0_{φ}, N^0_{θ} and $N^0_{\varphi\theta}$ are the initial force resultants due to the external pressure p defined as (Su *et al.* 2014 c)

$$N^0_{\varphi\varphi} = -\frac{pR}{2}\left(1 - \frac{\sin^2\varphi_1}{\sin^2\varphi}\right),\quad N^0_{\theta\theta} = -\frac{pR}{2}\left(1 + \frac{\sin^2\varphi_1}{\sin^2\varphi}\right), \qquad N^0_{\varphi\theta} = 0 \tag{15}$$

Now, the energy functional of FG spherical panel is introduced as

$$\Pi = U + U_f + U_e - T \tag{16}$$

3. Solution procedure

The Rayleigh-Ritz method is implemented to solve the problem. Considering appropriate analytical functions for displacement and rotation components is one of the most significant issues to obtain the proper accuracy. The survey of the literature shows the employment of different kinds of approximate functions. In this study, the vibration and buckling mode shapes of the FG spherical panels for different boundary supports are approximated using the beam displacement functions as follows

$$\begin{aligned} u_0(\varphi,\theta,t) &= \mathcal{U}\frac{\partial\Phi(\varphi)}{\partial\varphi}\Psi(\theta)e^{i\omega t}, \\ v_0 &= \mathcal{V}\,\Phi(\varphi)\frac{\partial\Psi(\theta)}{\partial\theta}e^{i\omega t}, \\ w_0 &= \mathcal{W}\,\Phi(\varphi)\Psi(\theta)e^{i\omega t}, \\ \psi_0 &= \mathcal{S}\,\frac{\partial\Phi(\varphi)}{\partial\varphi}\Psi(\theta)e^{i\omega t}, \\ \phi_0 &= \mathcal{P}\,\Phi(\varphi)\frac{\partial\Psi(\theta)}{\partial\theta}e^{i\omega t} \end{aligned} \tag{17}$$

in which $\mathcal{U}$, $\mathcal{V}$, $\mathcal{W}$, $\mathcal{S}$ and $\mathcal{P}$ are the constant parameters and ω stands for the natural frequency. In addition, $\Phi(\varphi)$ and $\Psi(\theta)$ are the displacement beam functions in φ and θ directions defined as

$$\Phi(\varphi) = a_1\cosh\left(\frac{\lambda_m\varphi}{\varphi_l}\right) + a_2\cos\left(\frac{\lambda_m\varphi}{\varphi_l}\right) - \xi_m\left[a_3\sinh\left(\frac{\lambda_m\varphi}{\varphi_l}\right) + a_4\sin\left(\frac{\lambda_m\varphi}{\varphi_l}\right)\right], \tag{18}$$

$$\Psi(\theta) = a_1 \cosh\left(\frac{\lambda_n \theta}{\theta_1}\right) + a_2 \cos\left(\frac{\lambda_n \theta}{\theta_1}\right) - \xi_n \left[a_3 \sinh\left(\frac{\lambda_n \theta}{\theta_1}\right) + a_4 \sin\left(\frac{\lambda_n \theta}{\theta_1}\right)\right]$$

where $a_i (i = 1,2,3,4)$, $\lambda_i (i = m, n)$ and $\xi_i (i = m, n)$ are given in Table 1 for different boundary conditions. Note that m is the half wave number in the axial direction and n is the circumferential wave number.

Substituting Eq. (17) into (16) and minimizing the energy functional with respect to unknown constant parameters as

$$\frac{\partial \Pi}{\partial \mathcal{U}} = \frac{\partial \Pi}{\partial \mathcal{V}} = \frac{\partial \Pi}{\partial \mathcal{W}} = \frac{\partial \Pi}{\partial \mathcal{S}} = \frac{\partial \Pi}{\partial \mathcal{P}} = 0 \tag{19}$$

result in the following governing equation

$$\left(\mathbf{K} - p\mathbf{K}_g - \omega^2 \mathbf{M}\right)\mathbf{X} = \mathbf{0} \tag{20}$$

where $\mathbf{K}$, $\mathbf{K}_g$ and $\mathbf{M}$ are the elastic stiffness matrix, geometrical stiffness matrix and mass matrix, respectively. Note that in the case of buckling analysis, the effect of the mass matrix is neglected. The eigenvalue problem of Eq. (20) has five conjugate solutions for each value of m and n. Each of these eigenvalues and corresponding eigenvectors relates to different displacement components. On the other hand, the eigenvalues should be minimized with respect to m and n values (Wave numbers in half-axial and circumferential directions, respectively) to obtain the critical buckling load and fundamental natural frequency.

4. Results and discussion

The FG spherical panel is made of Aluminum and Alumina respectively as the metal (m) and ceramic (c) phases. The inner surface is full of metal while the outer surface is ceramic rich. The material properties of Aluminum and Alumina including Young's modulus, Poisson's ratio and mass density are provided as follows (Su *et al*. 2014 c)

$$E_m = 70 \text{ GPa}, \quad \nu_m = 0.3, \quad \rho_m = 2707 \text{ kg/m}^3,$$
$$E_c = 380 \text{ Gpa}, \quad \nu_c = 0.3, \quad \rho_c = 5700 \text{ kg/m}^3$$

Various sets of boundary supports including clamped (C), simply-supported (S) and free (F) are considered at the edges of the panel. For example, SSCC indicates that the edges at $\theta = 0, \theta_1$ are simply supported and the other two edges are clamped. In order to account the impacts of the elastic medium, the following non-dimensional Winkler and Pasternak coefficients are considered

$$k_w = \frac{K_w R^4}{D_m}, \quad k_g = \frac{K_g R^2}{D_m}, \quad D_m = \frac{E_m h^3}{12(1 - \nu_m^2)}$$

In order to obtain the numerical results, the radius of the spherical panel is considered to be $R = 1$ m.

Diverse comparative results are given to demonstrate the accuracy of the presented study. In the first case, the critical buckling pressure of the FG spherical panel is compared in Table 2 with the results reported in (Bich and Phuong 2013). In the next, the comparison for the non-dimensional

Table 1 Value of a_i, λ_i and ξ_i for different boundary conditions

BC	$a_i (i = 1,2,3,4)$	$\lambda_i (i = m, n)$	$\xi_i (i = m, n)$
Simply supported- Simply supported	$a_1 = a_2 = a_3 = 0$, $a_4 = -1$	$i\pi$	1
Clamped-Clamped	$a_1 = a_3 = 1$, $a_2 = a_4 = -1$	$\cos\lambda_i \cosh\lambda_i = 1$	$\frac{\cosh\lambda_i - \cos\lambda_i}{\sinh\lambda_i - \sin\lambda_i}$
Clamped- Simply supported	$a_1 = a_3 = 1$, $a_2 = a_4 = -1$	$\tan\lambda_i = \tanh\lambda_i$	$\frac{\cosh\lambda_i - \cos\lambda_i}{\sinh\lambda_i - \sin\lambda_i}$

Table 2 Comparison of the critical buckling pressure ($10 \times$ MPa) of SSSS FG spherical panel ($R = 1, \varphi_0 = 11.537, \varphi_1 = 30^\circ, \theta_1 = 15^\circ$)

k		R/h		
		1000	1200	1500
0	Present study	3.870	2.758	1.684
	Bich and Phuong (2013)	3.929	2.640	1.698
	Error (%)	1.502	4.470	0.824
1	Present study	2.196	1.485	0.908
	Bich and Phuong (2013)	2.114	1.443	0.945
	Error (%)	3.879	2.911	3.915
5	Present study	1.306	0.905	0.555
	Bich and Phuong (2013)	1.294	0.868	0.556
	Error (%)	0.927	4.263	0.180
10	Present study	1.097	0.779	0.480
	Bich and Phuong (2013)	1.127	0.748	0.473
	Error (%)	2.662	4.144	1.480

Table 3 Comparisons of Non-dimensional frequencies $\Omega = \omega R^2\sqrt{\rho h/D}$ of isotropic spherical panel with different boundary condition ($R = 1$ m$, \theta_1 = 0.1, \varphi_1 = \frac{\pi-\theta_1}{2}, \varphi_2 = \frac{\pi+\theta_1}{2}, E = 70$ GPa$, \nu = 0.3, \rho = 2700$ kg/m^3)

BC		Mode Number				
		1	2	3	4	5
SSSS	Su *et al.* (2014 c)	1750.700	3216.600	3220.400	3817.000	3817.200
	Present study	1750.500	3217.500	3220.500	3817.200	3818.600
	Error (%)	0.011	0.028	0.003	0.005	0.037
SSCC	Su *et al.* (2014 c)	2242.200	3220.400	3987.500	4462.500	5675.700
	Present study	2242.000	3217.500	3988.600	4462.100	5673.800
	Error (%)	0.009	0.090	0.028	0.009	0.033
SSFF	Su *et al.* (2014 c)	897.400	1406.200	2441.800	2916.600	3126.400
	Present study	898.200	1408.000	2440.000	2917.500	3131.600
	Error (%)	0.089	0.128	0.074	0.031	0.166

Table 4 The non-dimensional fundamental frequencies $\Omega = \omega R^2\sqrt{\rho h/D_m}$ of FG spherical panel with various boundary conditions and subtended angle ($R = 1, \varphi_1 = 45^\circ, \frac{h}{R} = 0.1, \theta_1 = 60^\circ, E_m = 70\ GPa, \nu_m = 0.3, \rho_m = 2707\frac{Kg}{m^3}, E_c = 168\ GPa, \nu_c = 0.3, \rho_c = 5700\frac{Kg}{m^3},$)

φ_2	k		Boundary condition		
			CCCC	SSSS	CCSS
90	0.5	Present study	64.85	41.09	48.11
		Su *et al.* (2014 c)	64.63	41.03	48.21
		Error (%)	0.340	0.146	0.207
	1	Present study	64.25	40.7	47.66
		Su *et al.* (2014 c)	64.14	40.73	47.85
		Error (%)	0.171	0.074	0.397
	20	Present study	63.530	40.100	47.060
		Su *et al.* (2014 c)	63.200	39.990	47.090
		Error (%)	0.522	0.275	0.064
135	0.5	Present study	50.670	34.660	48.110
		Su *et al.* (2014 c)	50.630	33.380	48.210
		Error (%)	0.079	3.835	0.207
	1	Present study	50.200	34.330	47.660
		Su *et al.* (2014 c)	50.250	33.130	47.850
		Error (%)	0.100	3.622	0.397
	20	Present study	49.670	33.340	47.060
		Su *et al.* (2014 c)	49.530	32.080	47.020
		Error (%)	0.283	3.928	0.085

frequencies of isotropic and FG spherical panels is performed in Tables 3 and 4 for different boundary conditions. As observed, the numerical results have an excellent agreement that shows the correctness of the proposed formulation. In the following, various numerical results are provided to analyze the mechanical behavior of FG spheres.

The effects of the elastic medium on the critical buckling pressure of FG spherical panel were investigated in Table 5 for diverse boundary supports, subtended angles and circumferential angles. It is found that the existence of the elastic medium makes the panel more stable and increases the buckling pressure. The elastic medium has more impacts on the buckling pressure of SSSS panel in comparison to the other types of edge supports. In addition, results indicated that the effects of the elastic medium on the buckling pressure are more considerable for the panel with the larger subtended and circumferential angles. In other words, the rise of ϕ_2 and θ_1 highlights the influences of the elastic medium.

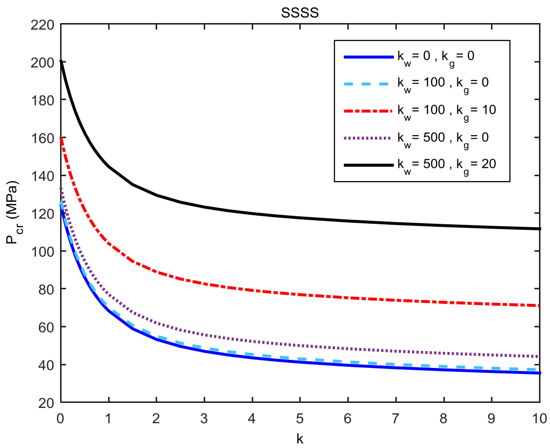

Fig. 2 Critical buckling pressure of SSSS FG spherical panel versus power-law index for various elastic foundation coefficient ($\varphi_1 = 45^{\circ}, \varphi_2 = 90^{\circ}, \theta_1 = 45^{\circ}, \frac{h}{R} = 0.02$)

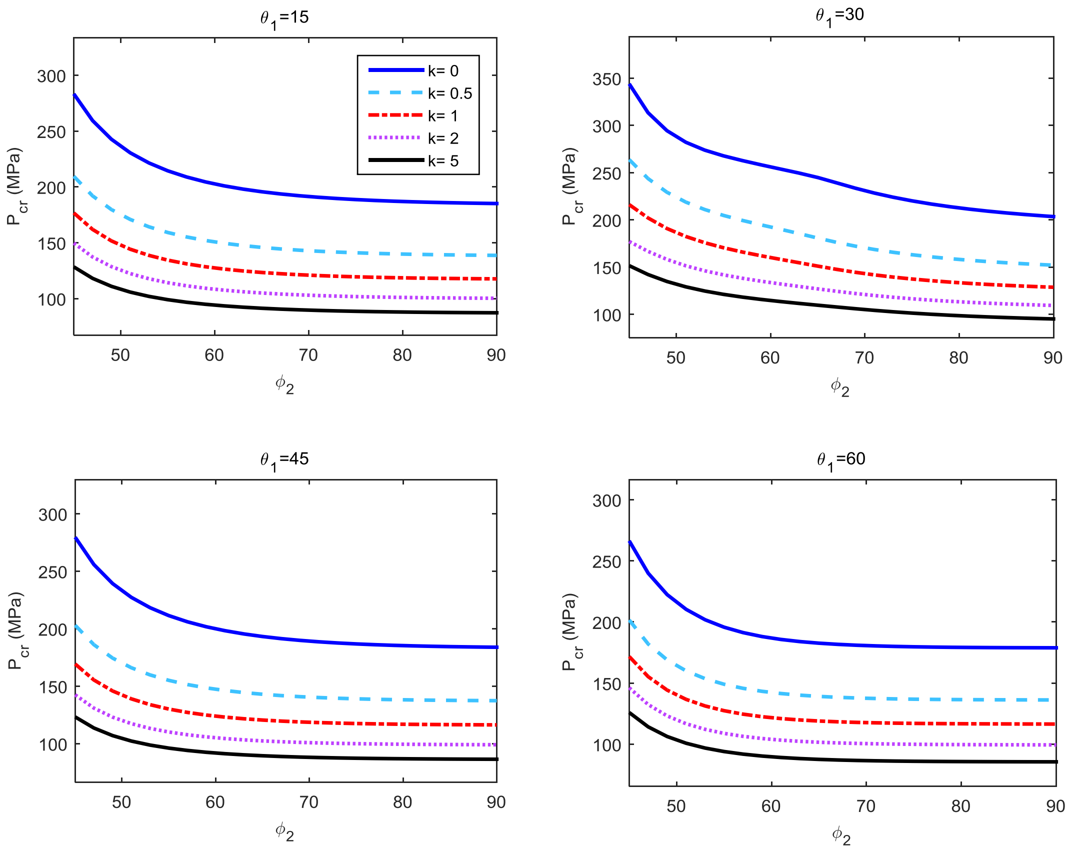

Fig. 3 Critical buckling pressures of SSSS FG spherical panel versus subtended angle (φ_2) for various power-law index and circumferential angle (θ_1). ($\varphi_1 = 30^{\circ}, (k_w, k_g) = (100,10), \frac{h}{R} = 0.02$).

The effects of the elastic medium on the variations of buckling pressure versus the power-law index are reported in Fig. 2. The SSSS FG spherical panel with the geometrical parameters of $\varphi_1 = 45^{\circ}, \varphi_2 = 90^{\circ}, \theta_1 = 45^{\circ}, h/R = 0.02$ is considered. It is generally observed that the rise of the power-law index reduces the buckling capacity and tends the critical pressures to the lower values. A comparison of the results for Winkler and Pasternak coefficients implies that the shear coefficient of the elastic medium has a more considerable effect on the buckling pressure. In addition, it is apparent that by the enhancement of the foundation coefficients, the impacts of the power-law index decrease.

On the other hand, one can see that the effects of the elastic foundation on the critical buckling pressure are still significant for higher values of the FG index. Note that considering the Pasternak coefficient of elastic medium considerably increases the critical buckling pressure.

The variations of the buckling pressure of fully simply-

Table 5 The effect of elastic foundation on critical buckling pressure (MPa) of FG spherical panel for various boundary conditions ($\varphi_1 = 30, k = 1, \frac{h}{R} = 0.02$)

φ_2	θ_1	$(k_w, k_g) = (0,0)$			$(k_w, k_g) = (100,10)$			$(k_w, k_g) = (200,20)$		
		CCCC	SSSS	SSCC	CCCC	SSSS	SSCC	CCCC	SSSS	SSCC
45	30	211.08	173.78	196.76	249.65	216.21	232.58	288.01	251.91	267.97
	60	167.46	125.60	166.58	209.20	171.78	206.81	249.04	217.23	244.35
	90	159.88	122.08	159.07	201.56	165.69	200.94	241.69	209.07	239.53
	120	157.37	121.83	156.63	198.97	164.41	198.67	239.22	206.79	237.77
60	30	142.68	118.10	121.83	180.67	160.46	162.71	218.19	199.41	201.51
	60	92.73	81.61	85.08	132.45	121.71	126.05	171.74	161.66	166.76
	90	87.02	79.65	82.89	126.42	118.64	122.54	165.33	157.43	161.95
	120	84.61	79.83	82.99	124.35	118.46	122.16	163.25	156.82	161.07
90	30	115.10	87.26	88.18	157.69	128.66	130.00	199.15	169.03	170.73
	60	84.05	76.81	78.13	123.85	116.52	118.43	163.13	155.99	158.41
	90	78.53	74.61	75.44	118.10	113.60	114.95	157.12	152.25	154.11
	120	76.74	74.41	75.03	116.26	113.25	114.35	155.20	151.66	153.25

Table 6 The effect of elastic foundation on the frequencies (Hz) of CCCC FG spherical panel ($\varphi_1 = 30^{\circ}, k = 1, \frac{h}{R} = 0.05$)

φ_2	θ_1	$(k_w, k_g) = (0,0)$				$(k_w, k_g) = (200,15)$			
		ω_1	ω_2	ω_3	ω_4	ω_1	ω_2	ω_3	ω_4
60	30	3306.1	4710.4	6095.0	7030.2	3853.2	5401.8	6817.7	7828.4
	60	2213.3	2768.2	3610.8	3917.4	2671.2	3373.2	4270.2	4633.7
	90	2089.7	2204.3	2604.3	3315.5	2509.7	2727.1	3228.1	4014.2
	120	2051.8	2064.1	2228.7	2563.7	2465.8	2539.0	2765.9	3191.6
90	30	2305.3	2609.9	3222.8	3979.9	2765.0	3174.1	3867.0	4644.7
	60	1629.6	1672.2	1786.1	2207.9	2006.9	2133.3	2292.6	2829.9
	90	1442.3	1447.6	1515.6	1735.3	1841.8	1844.0	1939.7	2252.1
	120	1360.7	1371.2	1401.6	1576.5	1714.0	1747.4	1840.8	2006.8
120	30	2099.1	2157.1	2440.0	2764.3	2524.0	2657.9	2995.4	3389.9
	60	1387.8	1465.6	1544.4	1722.9	1760.7	1857.8	2002.1	2135.8
	90	1195.8	1260.6	1313.9	1408.3	1513.7	1586.3	1695.8	1856.7
	120	1103.8	1186.3	1218.8	1295.4	1398.8	1436.6	1565.9	1684.3

supported FG spherical panel versus subtended angles for variant power-law indexes and circumferential angles are demonstrated in Fig. 3. One can see that the rise of the subtended angle decreases the buckling pressure. This reduction is more remarkable for the lower values of the power-law index.

In addition, results reveal that in most of the cases, for the subtended angles larger than $\phi_2 > 70$, the buckling pressure does not considerably change. The first four natural frequencies of the fully clamped FG spherical panel are presented in Table 6 for two different elastic medium coefficients and several subtended and circumferential angles. It is concluded that the FG panel with the larger circumferential angle has a lower frequency. To give some more details, the first six vibrational mode shapes of the FG spherical panel are demonstrated in Fig. 4. Moreover, the effects of the elastic medium on the natural frequencies ofsimply-supported FG panel are reported in Table 7 for diverse thickness-radius ratios, circumferential angles and power-law indexes. It is evident that the effects of the elastic medium on the buckling pressure of the thinner panel are more significant. In addition, it can be seen that by the increase of Winkler and Pasternak coefficients of the elastic medium, the impacts of elastic medium decrease.

The effects of the elastic medium on the variations of natural frequencies of the FG spherical panel versus subtended angle are illustrated in Fig. 5 for four different circumferential angles ($\theta_1 = 15, 13, 45, 60$). It is clearly seen that the existence of elastic medium results in the higher natural frequencies. In addition, different reduction trends were observed for various circumferential angles. In the case of $\theta_1 = 15$, the uniform reduction of frequencies is found with the increase of ϕ_2. However, in the case of $\theta_1 = 60$, one can see the higher rate of reduction for $40 < \phi_2 < 60$.

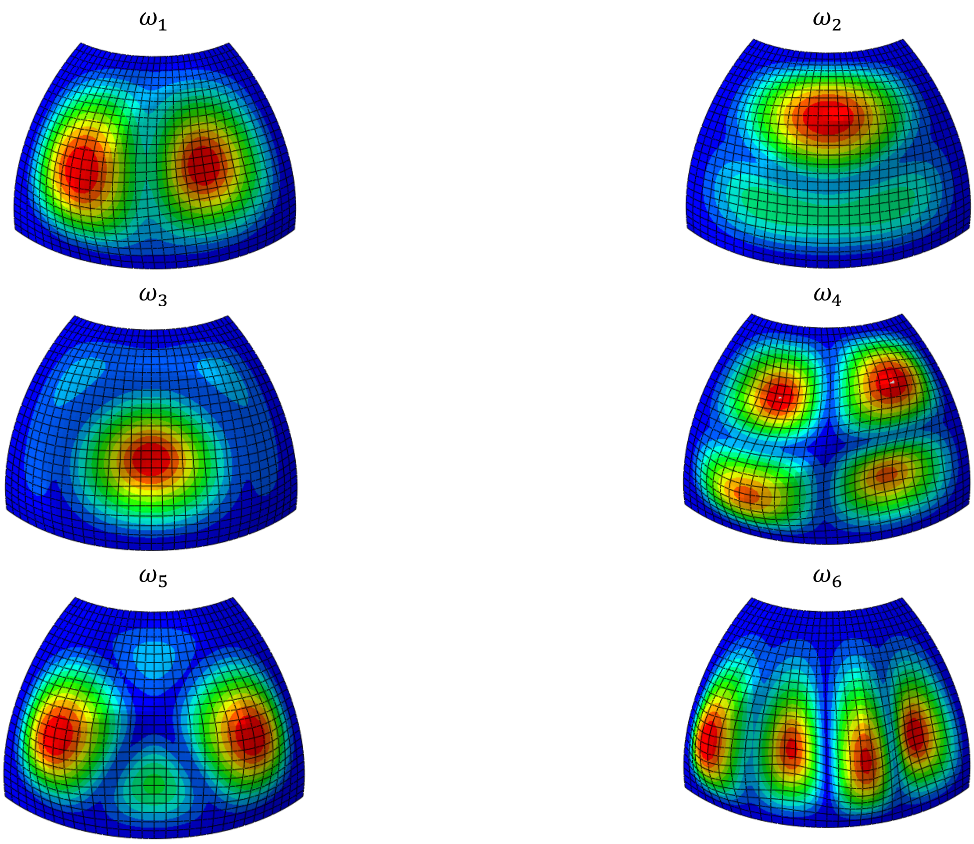

Fig. 4 First six vibrational mode shapes of CCCC FG spherical panel
$(\varphi_1 = 30^{\circ}, \varphi_2 = 90^{\circ}, \theta_1 = 90^{\circ}, k = 1, \frac{h}{R} = 0.05, (k_w, k_g) = (0,0))$

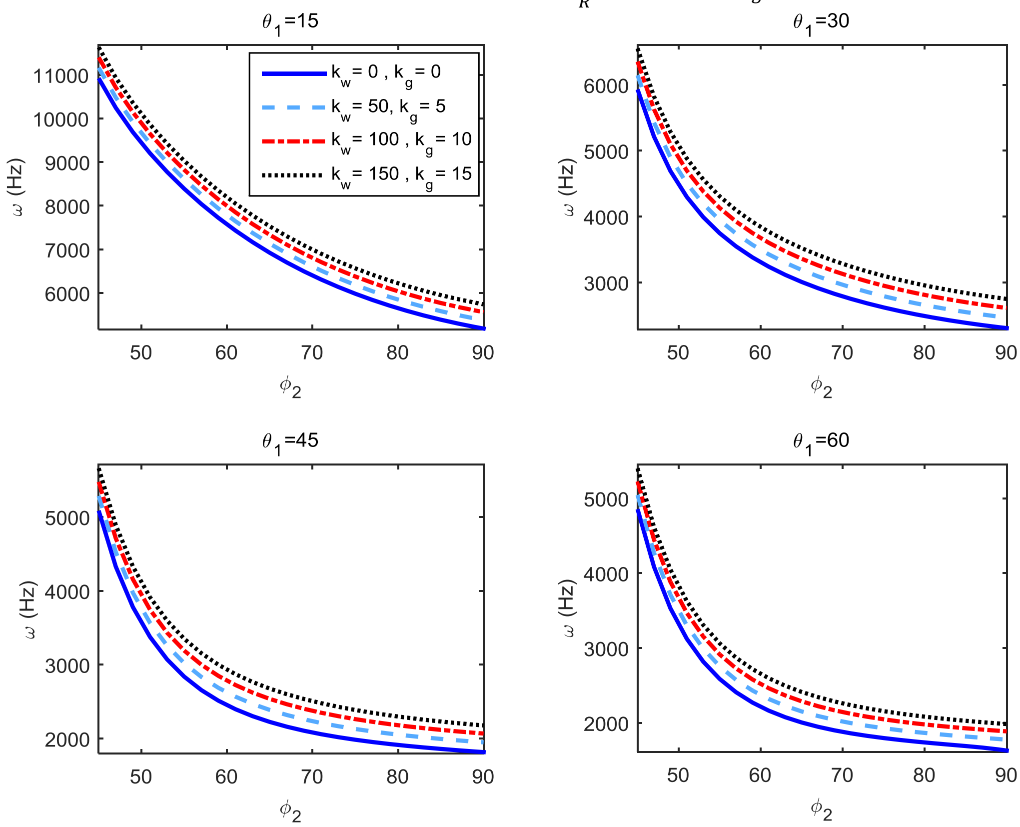

Fig 5 The fundamental frequency (Hz) of CCCC FG spherical panel versus subtended angle (φ_2) for various elastic foundation coefficient and subtended angle (θ_1) ($\varphi_1 = 30^{\circ}, k = 1, \frac{h}{R} = 0.05$)

Table 7 The effect of elastic foundation on the fundamental frequency (Hz) of SSSS FG spherical panel for various thickness to radius ratio ($\varphi_1 = 45^\circ, \varphi_2 = 90^\circ$)

θ_1	k	$(k_w, k_g) = (0,0)$			$(k_w, k_g) = (200,0)$			$(k_w, k_g) = (200,20)$		
		$\frac{h}{R}=0.02$	$\frac{h}{R}=0.04$	$\frac{h}{R}=0.06$	$\frac{h}{R}=0.02$	$\frac{h}{R}=0.04$	$\frac{h}{R}=0.06$	$\frac{h}{R}=0.02$	$\frac{h}{R}=0.04$	$\frac{h}{R}=0.06$
15	0	1953.75	3007.56	4034.12	1981.86	3043.47	4073.38	2439.71	3637.16	4731.94
	0.5	1797.46	2714.13	3608.42	1834.10	2761.41	3659.94	2408.91	3513.53	4492.91
	1	1698.50	2539.80	3356.67	1741.54	2595.49	3417.14	2397.75	3455.87	4366.67
	5	1501.94	2286.88	3011.53	1564.78	2365.95	3096.45	2443.97	3497.96	4325.43
30	0	1527.67	1714.13	1951.10	1562.62	1775.31	2030.51	1762.95	2100.70	2445.46
	0.5	1434.26	1613.10	1825.93	1479.08	1690.66	1926.41	1733.09	2091.87	2433.17
	1	1365.67	1538.88	1739.01	1418.05	1628.83	1855.13	1710.20	2083.57	2424.70
	5	1165.25	1333.46	1525.94	1244.17	1465.50	1692.83	1644.73	2075.29	2435.23
60	0	1444.42	1661.27	1748.44	1481.33	1724.16	1836.12	1702.67	1908.93	2060.89
	0.5	1350.52	1556.26	1658.76	1397.94	1636.96	1769.31	1656.66	1877.41	2050.16
	1	1285.33	1478.52	1585.18	1340.73	1572.75	1713.27	1621.88	1849.97	2033.68
	5	1099.15	1268.53	1361.04	1182.35	1408.31	1549.00	1504.96	1758.62	1968.00

Table 8 The effect of elastic foundation on the fundamental frequency (Hz) of FG spherical panel under external pressure P (MPa) ($\varphi_1 = 45^\circ, \varphi_2 = 90^\circ, \theta_1 = 90^\circ, \frac{h}{R} = 0.02$)

BC	k	$(k_w, k_g) = (0,0)$			$(k_w, k_g) = (100,5)$			$(k_w, k_g) = (200,10)$		
		$p=15$	$p=30$	$p=45$	$p=15$	$p=30$	$p=45$	$p=15$	$p=30$	$p=45$
CCCC	0.5	1316.41	1242.29	1129.31	1423.28	1364.01	1292.67	1517.50	1466.31	1408.64
	1	1233.27	1126.56	947.20	1361.18	1289.55	1188.92	1470.16	1410.80	1341.83
	2	1128.98	967.15	631.71	1286.57	1197.64	1048.67	1414.59	1344.91	1260.59
SSSS	0.5	1251.90	1223.42	1095.31	1360.09	1334.54	1274.32	1459.53	1430.45	1379.49
	1	1183.71	1111.51	897.94	1309.89	1267.99	1173.44	1423.62	1379.69	1319.57
	2	1098.52	932.83	594.59	1249.73	1181.61	1015.05	1376.31	1316.50	1243.50
SSCC	0.5	1292.30	1229.35	1109.00	1392.30	1339.82	1279.77	1480.72	1435.35	1384.64
	1	1214.48	1118.91	910.36	1333.12	1270.77	1182.14	1434.77	1382.90	1323.16
	2	1115.24	940.88	612.09	1260.45	1183.96	1025.49	1378.90	1319.18	1246.84
CCSS	0.5	1256.45	1227.92	1119.84	1365.03	1340.18	1285.74	1464.90	1441.73	1401.01
	1	1187.68	1121.10	935.45	1314.30	1281.01	1181.95	1428.66	1398.98	1336.92
	2	1101.82	961.35	614.02	1253.63	1193.88	1040.94	1386.80	1339.66	1256.24

The impacts of external pressure on the natural frequencies of FG spherical panel are given in Table 8 for various elastic medium coefficients, power-law indexes and boundary supports. As expected, the increase of external pressure lessens the natural frequencies. The numerical results indicate that increasing the elastic medium coefficients reduces the influences of external pressure on the natural frequencies. In addition, one can see that the fully clamped and simply-supported boundary conditions result in the highest and lowest frequencies, respectively.

The changes of fundamental frequencies of fully clamped FG panel against the external pressure are demonstrated in Fig. 6 for different power-law indexes and circumferential angles. It is found that the rise of external pressure significantly decreases the frequency. Almost the same trends are observed for different circumferential angles. In addition, a comparison of the results for various power-law indexes shows the higher rate of reduction (slope) in frequency for the larger k.

The variations of the frequencies of simply-supported FG Panel versus external pressure are exhibited in Fig. 7 for diverse elastic medium coefficients and subtended angles. It is obvious that increasing the subtended angle reduces the influences of external pressure on the fundamental frequency. Since the existence of the elastic medium improves the stability of the panel, the fewer effects of external pressure on the fundamental frequencies are observed for the larger values of the elastic medium coefficients.

5. Conclusion

The vibration and buckling analysis of FG spherical panels resting of elastic medium under external pressure was highlighted in this study. The continuous variation of material properties along the thickness direction was regarded for the FG sphere. On the basis of FSDT and employing the Ritz method the governing equations were

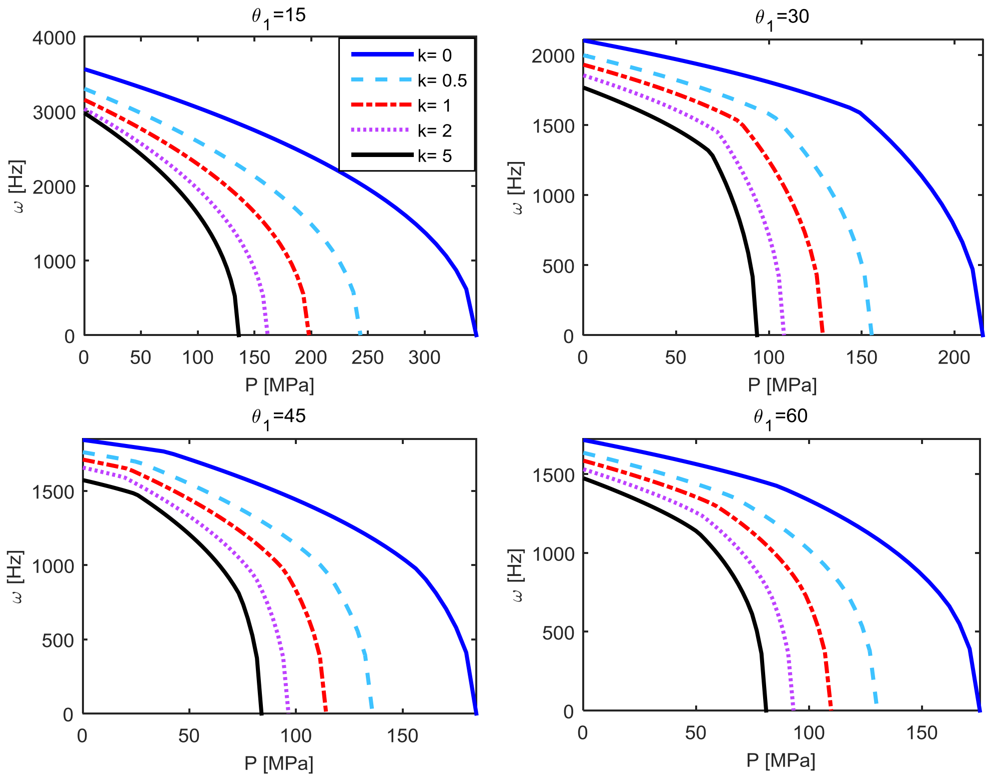

Fig 6 The fundamental frequency (Hz) of CCCC FG spherical panel versus external pressure for various power law index and subtended angle (θ_1) $(\varphi_1 = 45^{\circ}, \varphi_2 = 90^{\circ}, (k_w, k_g) = (100,10), \frac{h}{R} = 0.02)$

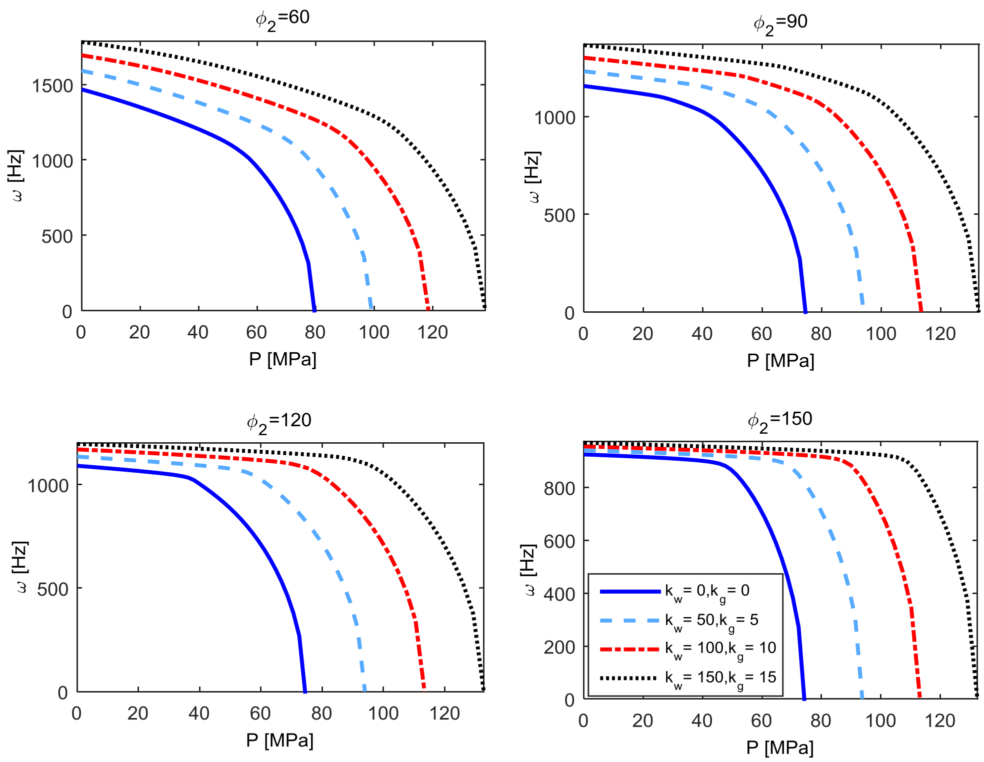

Fig 7 The fundamental frequency (Hz) of SSSS FG spherical panel versus external pressure for various elastic foundation coefficient and subtended angle (φ_2) $(\varphi_1 = 90^{\circ}, \theta_1 = 90^{\circ}, k = 1, \frac{h}{R} = 0.02)$

obtained. The beam functions in two-dimensions were used to approximate displacement components. Different results were comparatively presented to check the accuracy of the presented model. A wide range of results was given to examine the mechanical behavior of embedded FG spherical panels under external pressure. It was concluded that the FG panels with larger power-law index, subtended and circumferential angles have the lower fundamental frequencies and buckling pressures. It was also found that the elastic medium increases frequency and buckling pressure. Moreover, the results revealed that external pressure reduces the fundamental frequencies. In addition, it was concluded that the increase of power-law index and subtended angle respectively increases and decreases the effect of external pressure on the fundamental frequency.

Acknowledgements

This paper is supported by Shaanxi Key Research and Development Plan (Grant: 2018ZDXM-GY-077), Shaanxi Natural Science Basic Research Project (Grant: S2019-JC-YB-2897), Project of Joint Postgraduate Training Base of Xi'an Technological University, and Research Project of Graduate Education and Teaching Reform of Xi'an Technological University in 2017.

References

ACI 228.2R-13. (2013), “Nondestructive test methods for evaluation of concrete in structures”, *American Concrete Institute Report*, Farmington Hills, U.S.A.

Akgoz, B., and Civalek, O. (2011), “Nonlinear vibration analysis of laminated plates resting on nonlinear two-parameters elastic foundations”, *Steel Compos. Struct.*, **11**(5), 403-421. https://doi.org/10.12989/scs.2011.11.5.403.

Alijani, F., Amabili, M., Karagiozis, K., and Bakhtiari-Nejad, F. (2011), “Nonlinear vibrations of functionally graded doubly curved shallow shells”, *J. Sound Vib.*, **330**(7), 1432-1454. https://doi.org/10.1016/j.jsv.2010.10.003.

Ansari, R., and Torabi, J. (2016), “Numerical study on the buckling and vibration of functionally graded carbon nanotube-reinforced composite conical shells under axial loading”, *Compos. Part B Eng.*, **95**, 196-208. https://doi.org/10.1016/j.compositesb.2016.03.080.

Ansari, R., Torabi, J., and Shojaei, M. F. (2016), “Vibrational analysis of functionally graded carbon nanotube-reinforced composite spherical shells resting on elastic foundation using the variational differential quadrature method”, *Europe J. Mech. A/Solids*, **60**, 166-182. https://doi.org/10.1016/j.euromechsol.2016.07.003.

Bich, D. H., and Van Tung, H. (2011), “Non-linear axisymmetric response of functionally graded shallow spherical shells under uniform external pressure including temperature effects”., *J Non-Linear Mech.*, **46**(9), 1195-1204. https://doi.org/10.1016/j.ijnonlinmec.2011.05.015.

Bich, D. H., Van Dung, D., and Nam, V. H. (2013), “Nonlinear dynamic analysis of eccentrically stiffened imperfect functionally graded doubly curved thin shallow shells”, *Compos. Struct.*, **96**, 384-395.https://doi.org/10.1016/j.compstruct.2012.10.009

Bich, D. H., and Phuong, N. T. (2013), “Buckling Analysis of Functionally Graded Annular Spherical Shells and Segments Subjected to Mechanic Loads”, *VNU J. Sci. Mathematics-Physics*, **29**(3), https://js.vnu.edu.vn/MaP/article/view/869.

Civalek, O., and Ülker, M. (2004), “Harmonic differential quadrature (HDQ) for axisymmetric bending analysis of thin isotropic circular plates”, *Struct. Eng. Mech.*, **17**(1), 1-14. https://doi.org/10.12989/sem.2004.17.1.001.

Civalek, O. (2006), “Free vibration analysis of composite conical shells using the discrete singular convolution algorithm”, *Steel Compos. Struct.*, **6**(4), 353. https://doi.org/10.12989/scs.2006.6.4.353.

Civalek, O. (2007), “Linear vibration analysis of isotropic conical shells by discrete singular convolution (DSC)”, *Struct. Eng. Mech.*, **25**(1), 127-130. https://doi.org/10.12989/sem.2007.25.1.127.

Civalek, Ö., and Acar, M. H. (2007), “Discrete singular convolution method for the analysis of Mindlin plates on elastic foundations”, *J. Pressure Vessels Piping*, **84**(9), 527-535. https://doi.org/10.1016/j.ijpvp.2007.07.001.

Civalek, Ö. (2008), “Vibration analysis of conical panels using the method of discrete singular convolution”, *Communications Numerical Methods Eng.*, **24**(3), 169-181. https://doi.org/10.1002/cnm.961.

Darilmaz, K. (2017), “Static and free vibration behaviour of orthotropic elliptic paraboloid shells”, *Steel Compos. Struct.*, **23**(6), 737-746. https://doi.org/10.12989/scs.2017.23.6.737.

Foroughi, H., and Azhari, M. (2014), “Mechanical buckling and free vibration of thick functionally graded plates resting on elastic foundation using the higher order B-spline finite strip method”, *Meccanica*, **49**(4), 981-993. https://doi.org/10.1007/s11012-013-9844-2.

Foroutan, K., Shaterzadeh, A., and Ahmadi, H. (2018), “Nonlinear dynamic analysis of spiral stiffened functionally graded cylindrical shells with damping and nonlinear elastic foundation under axial compression”, *Struct. Eng. Mech.*, **66**(3), 295-303. http://dx.doi.org/10.12989/sem.2018.66.3.295.

Ganapathi, M. (2007), “Dynamic stability characteristics of functionally graded materials shallow spherical shells”, *Compos. Struct.*, **79**(3), 338-343. https://doi.org/10.1016/j.compstruct.2006.01.012.

Ghannad, M., Nejad, M. Z., Rahimi, G. H., and Sabouri, H. (2012), “Elastic analysis of pressurized thick truncated conical shells made of functionally graded materials”, *Struct. Eng. Mech.*, **43**(1), 105-126. https://doi.org/10.12989/sem.2012.43.1.105.

Hasrati, E., Ansari, R., and Torabi, J. (2018), “A novel numerical solution strategy for solving nonlinear free and forced vibration problems of cylindrical shells”, *Appl. Math. Modelling*, **53**, 653-672. https://doi.org/10.1016/j.apm.2017.08.027.

Heydarpour, Y., Aghdam, M. M., and Malekzadeh, P. (2014), “Free vibration analysis of rotating functionally graded carbon nanotube-reinforced composite truncated conical shells”, *Compos. Struct.*, **117**, 187-200.https://doi.org/10.1016/j.compstruct.2014.06.023.

Jung, W. Y., Han, S. C., Lee, W. H., and Park, W. T. (2016), “Postbuckling analysis of laminated composite shells under shear loads”, *Steel Compos. Struct.*, **21**(2), 373-394. https://doi.org/10.12989/scs.2016.21.2.373.

Kar, V. R., and Panda, S. K. (2015), “Large deformation bending analysis of functionally graded spherical shell using FEM”, *Struct. Eng. Mech.*, **53**(4), 661-679. http://dx.doi.org/10.12989/sem.2015.53.4.661.

Karroubi, R., and Irani-Rahaghi, M. (2019), “Rotating sandwich cylindrical shells with an FGM core and two FGPM layers: free vibration analysis”, *Appl. Math. Mech.*, **40**(4), 563-578. https://doi.org/10.1007/s10483-019-2469-8.

Khayat, M., Poorveis, D., and Moradi, S. (2016), “Buckling analysis of laminated composite cylindrical shell subjected to lateral displacement-dependent pressure using semi-analytical finite strip method”, *Steel Compos. Struct.*, **22**(2), 301-321. https://doi.org/10.12989/scs.2016.22.2.301.

Loy, C. T., Lam, K. Y., and Reddy, J. N. (1999), “Vibration of functionally graded cylindrical shells”, *J. Mech. Sci.*, **41**(3), 309-324. https://doi.org/10.1016/S0020-7403(98)00054-X.

Mao, Y. Q., Fu, Y. M., Chen, C. P., and Li, Y. L. (2011), “Nonlinear dynamic response for functionally graded shallow spherical shell under low velocity impact in thermal environment”, *Appl. Math. Modelling*, **35**(6), 2887-2900. https://doi.org/10.1016/j.apm.2010.12.012.

Mercan, K., Demir, Ç., and Civalek, Ö. (2016), “Vibration analysis of FG cylindrical shells with power-law index using discrete singular convolution technique”, *Curved Layered Struct.*, **3**(1), 2353-7396. https://doi.org/10.1515/cls-2016-0007 .

Naghsh, A., Saadatpour, M. M., and Azhari, M. (2015), “Free vibration analysis of stringer stiffened general shells of revolution using a meridional finite strip method”, *Thin-Walled Struct.*, **94**, 651-662. https://doi.org/10.1016/j.tws.2015.05.015.

Patel, B. P., Gupta, S. S., Loknath, M. S., and Kadu, C. P. (2005), “Free vibration analysis of functionally graded elliptical cylindrical shells using higher-order theory”, *Compos. Struct.*, **69**(3), 259-270. https://doi.org/10.1016/j.compstruct.2004.07.002.

Shahsiah, R., Eslami, M. R., and Naj, R. (2006), “Thermal instability of functionally graded shallow spherical shell”, *J. Thermal Stresses*, **29**(8), 771-790. https://doi.org/10.1080/01495730600705406.

Shen, H. S., and Xiang, Y. (2012), “Nonlinear vibration of nanotube-reinforced composite cylindrical shells in thermal environments”, *Comput. Methods Appl. Mech. Eng.*, **213**, 196-205. https://doi.org/10.1016/j.cma.2011.11.025.

Sofiyev, A. H., Hui, D., Huseynov, S. E., Salamci, M. U., and Yuan, G. Q. (2016), “Stability and vibration of sandwich cylindrical shells containing a functionally graded material core with transverse shear stresses and rotary inertia effects”, *Proceedings of the Institution of Mechanical Engineers, Part C: Journal of Mechanical Engineering Science*, **230**(14), 2376-2389. https://doi.org/10.1177/0954406215593570.

Song, M. K., Kim, S. H., and Choi, C. K. (2006), “Enhanced finite element modeling for geometric non-linear analysis of cable-supported structures”, *Struct. Eng. Mech.*, **22**(5), 575-598. https://doi.org/10.12989/sem.2006.22.5.575.

Striz, A. G., Chen, W. L., and Bert, C. W. (1997), “Free vibration of plates by the high accuracy quadrature element method”, *J. Sound Vib.*, **202**(5), 689-702. https://doi.org/10.1006/jsvi.1996.0846.

Su, Z., Jin, G., Shi, S., Ye, T., and Jia, X. (2014a), “A unified solution for vibration analysis of functionally graded cylindrical, conical shells and annular plates with general boundary conditions”, *J. Mech. Sci.*, **80**, 62-80. https://doi.org/10.1016/j.ijmecsci.2014.01.002.

Su, Z., Jin, G., Shi, S., and Ye, T. (2014b), “A unified accurate solution for vibration analysis of arbitrary functionally graded spherical shell segments with general end restraints”, *Compos. Struct.*, **111**, 271-284.

Su, Z., Jin, G., and Ye, T. (2014c), “Free vibration analysis of moderately thick functionally graded open shells with general boundary conditions”, *Compos. Struct.*, **117**, 169-186. https://doi.org/10.1016/j.compstruct.2014.01.006.

Thomas, B., and Roy, T. (2016), “Vibration analysis of functionally graded carbon nanotube-reinforced composite shell structures”, *Acta Mechanica*, **227**(2), 581-599. https://doi.org/10.1007/s00707-015-1479-z.

Torabi, J., and Ansari, R. (2018), “Thermally induced mechanical analysis of temperature-dependent FG-CNTRC conical shells”, *Struct. Eng. Mech.*, **68**(3), 313-323. http://dx.doi.org/10.12989/sem.2018.68.3.313.

Torabi, J., and Ansari, R. (2018), “A higher-order isoparametric superelement for free vibration analysis of functionally graded shells of revolution”, *Thin-Walled Struct.*, **133**, 169-179. https://doi.org/10.1016/j.tws.2018.09.040.

Tornabene, F. (2009), “Free vibration analysis of functionally graded conical, cylindrical shell and annular plate structures with a four-parameter power-law distribution”, *Comput. Methods Appl. Mech. Eng.*, **198**(37-40), 2911-2935. https://doi.org/10.1016/j.cma.2009.04.011.

Wang, Q., Pang, F., Qin, B., and Liang, Q. (2018), “A unified formulation for free vibration of functionally graded carbon nanotube reinforced composite spherical panels and shells of revolution with general elastic restraints by means of the Rayleigh–Ritz method”, *Polymer Compos.*, **39**(S2), E924-E944. https://doi.org/10.1002/pc.24339.

Wu, Y., Xing, Y., and Liu, B. (2018), “Analysis of isotropic and composite laminated plates and shells using a differential quadrature hierarchical finite element method”, *Compos. Struct.*, **205**, 11-25. https://doi.org/10.1016/j.compstruct.2018.08.095

Xie, X., Zheng, H., and Jin, G. (2015), “Free vibration of four-parameter functionally graded spherical and parabolic shells of revolution with arbitrary boundary conditions”, *Compos. Part B Eng.*, **77**, 59-73. https://doi.org/10.1016/j.compositesb.2015.03.016.

Ye, T., Jin, G., and Su, Z. (2014), “Three-dimensional vibration analysis of laminated functionally graded spherical shells with general boundary conditions”, *Compos. Struct.*, **116**, 571-588. https://doi.org/10.1016/j.compstruct.2014.05.046.

CC

Appendix

The coefficients of the elastic stiffness matrix, mass matrix and geometrical stiffness matrix are presented in the Appendix.

- Elastic stiffness matrix

$$K_{11}=\int_0^{\theta_1}\int_{\varphi_1}^{\varphi_2}\Bigg\{A_{11}\Psi^2(\theta)\left[\left(\frac{\partial^2\Phi(\varphi)}{\partial\varphi^2}\right)^2\sin(\varphi)+\left(\frac{\partial\Phi(\varphi)}{\partial\varphi}\right)^2\frac{\cos^2(\varphi)}{\sin(\varphi)}\right]+2A_{12}\Psi^2(\theta)\frac{\partial^2\Phi(\varphi)}{\partial\varphi^2}\frac{\partial\Phi(\varphi)}{\partial\varphi}\cos(\varphi)+A_{66}\left(\frac{\kappa\sin^2(\varphi)+1}{\sin(\varphi)}\right)\left(\frac{\partial\Phi(\varphi)}{\partial\varphi}\right)^2\left(\frac{\partial\Psi(\theta)}{\partial\theta}\right)^2\Bigg\}d\varphi d\theta$$

$$K_{12}=\int_0^{\theta_1}\int_{\varphi_1}^{\varphi_2}\Bigg\{A_{11}\cos(\varphi)\Psi(\theta)\frac{\partial^2\Psi(\theta)}{\partial\theta^2}\frac{\partial\Phi(\varphi)}{\partial\varphi}\Phi(\varphi)+A_{12}\Psi(\theta)\frac{\partial\Psi^2(\theta)}{\partial\theta^2}\frac{\partial^2\Phi(\varphi)}{\partial\varphi^2}\Phi(\varphi)+A_{66}\left(\frac{\partial\Psi(\theta)}{\partial\theta}\right)^2\frac{\partial\Phi(\varphi)}{\partial\varphi}\left[\frac{\partial\Phi(\varphi)}{\partial\varphi}-\Phi(\varphi)\cot(\varphi)\right]\Bigg\}d\varphi d\theta$$

$$K_{13}=\int_0^{\theta_1}\int_{\varphi_1}^{\varphi_2}\Bigg\{A_{11}\cos(\varphi)\Psi^2(\theta)\frac{\partial\Phi(\varphi)}{\partial\varphi}\Phi(\varphi)+A_{12}\sin(\varphi)\Psi^2(\theta)\frac{\partial^2\Phi(\varphi)}{\partial\varphi^2}\Phi(\varphi)-A_{66}\sin(\varphi)\Psi^2(\theta)\left(\frac{\partial\Phi(\varphi)}{\partial\varphi}\right)^2\Bigg\}d\varphi d\theta$$

$$K_{14}=\int_0^{\theta_1}\int_{\varphi_1}^{\varphi_2}\Bigg\{-\kappa RA_{66}\sin(\varphi)\Psi^2(\theta)\left(\frac{\partial\Phi(\varphi)}{\partial\varphi}\right)^2+2B_{12}\Psi^2(\theta)\frac{\partial^2\Phi(\varphi)}{\partial\varphi^2}\frac{\partial\Phi(\varphi)}{\partial\varphi}\cos(\varphi)+B_{11}\Psi^2(\theta)\left[\left(\frac{\partial^2\Phi(\varphi)}{\partial\varphi^2}\right)^2\sin(\varphi)+\left(\frac{\partial\Phi(\varphi)}{\partial\varphi}\right)^2\frac{\cos^2(\varphi)}{\sin(\varphi)}\right]+\frac{2B_{66}}{\sin(\varphi)}\left(\frac{\partial\Psi(\theta)}{\partial\theta}\right)^2\left(\frac{\partial\Phi(\varphi)}{\partial\varphi}\right)^2\Bigg\}d\varphi d\theta$$

$$K_{15}=\int_0^{\theta_1}\int_{\varphi_1}^{\varphi_2}\Bigg\{B_{11}\cot(\varphi)\Psi(\theta)\frac{\partial^2\Psi(\theta)}{\partial\theta^2}\frac{\partial\Phi(\varphi)}{\partial\varphi}\Phi(\varphi)+B_{12}\Psi(\theta)\frac{\partial\Psi^2(\theta)}{\partial\theta^2}\frac{\partial^2\Phi(\varphi)}{\partial\varphi^2}\Phi(\varphi)+B_{66}\left(\frac{\partial\Psi(\theta)}{\partial\theta}\right)^2\frac{\partial\Phi(\varphi)}{\partial\varphi}\left[\frac{\partial\Phi(\varphi)}{\partial\varphi}-\Phi(\varphi)\cot(\varphi)\right],$$

$$K_{21}=K_{12},$$

$$K_{22}=\int_0^{\theta_1}\int_{\varphi_1}^{\varphi_2}\Bigg\{\frac{A_{11}}{\sin(\varphi)}\left(\frac{\partial^2\Psi(\theta)}{\partial\theta^2}\right)^2\Phi^2(\varphi)+A_{66}\left(\frac{\partial\Psi(\theta)}{\partial\theta}\right)^2\left[\left(\frac{\partial\Phi(\varphi)}{\partial\varphi}\right)^2\sin(\varphi)+\left(\frac{\kappa\sin^2(\varphi)+\cos^2(\varphi)}{\sin(\varphi)}\right)\Phi^2(\varphi)-\cos(\varphi)\Phi(\varphi)\frac{\partial\Phi(\varphi)}{\partial\varphi}\right]\Bigg\}d\varphi d\theta,$$

$$K_{23}=\int_0^{\theta_1}\int_{\varphi_1}^{\varphi_2}\Bigg\{A_{11}\frac{\partial^2\Psi(\theta)}{\partial\theta^2}\Psi(\theta)\Phi^2(\varphi)-\kappa A_{66}\left(\frac{\partial\Psi(\theta)}{\partial\theta}\right)^2\Phi^2(\varphi)\Bigg\}d\varphi d\theta$$

$$K_{24}=\int_0^{\theta_1}\int_{\varphi_1}^{\varphi_2}\Bigg\{B_{11}\cot(\varphi)\Psi(\theta)\frac{\partial^2\Psi(\theta)}{\partial\theta^2}\frac{\partial\Phi(\varphi)}{\partial\varphi}\Phi(\varphi)+B_{12}\Psi(\theta)\frac{\partial\Psi^2(\theta)}{\partial\theta^2}\frac{\partial^2\Phi(\varphi)}{\partial\varphi^2}\Phi(\varphi)+B_{66}\left(\frac{\partial\Psi(\theta)}{\partial\theta}\right)^2\frac{\partial\Phi(\varphi)}{\partial\varphi}\left[\frac{\partial\Phi(\varphi)}{\partial\varphi}-\Phi(\varphi)\cot(\varphi)\right],$$

$$K_{25}=\int_0^{\theta_1}\int_{\varphi_1}^{\varphi_2}\Bigg\{-\kappa RA_{66}\sin(\varphi)\left(\frac{\partial\Psi(\theta)}{\partial\theta}\right)^2\Phi(\varphi)^2+\frac{B_{11}}{\sin(\varphi)}\left(\frac{\partial^2\Psi(\theta)}{\partial\theta^2}\right)^2\Phi^2(\varphi)+B_{66}\left(\frac{\partial\Psi(\theta)}{\partial\theta}\right)^2\left[\left(\frac{\partial\Phi(\varphi)}{\partial\varphi}\right)^2\sin(\varphi)+\left(\frac{\cos^2(\varphi)}{\sin(\varphi)}\right)\Phi^2(\varphi)-2\cos(\varphi)\Phi(\varphi)\frac{\partial\Phi(\varphi)}{\partial\varphi}\right]\Bigg\}d\varphi d\theta,$$

$$K_{31}=K_{13},\qquad K_{32}=K_{23},$$

$$K_{33} = \int_0^{\theta_1}\int_{\varphi_1}^{\varphi_2} \left\{ A_{11}\sin(\varphi)\,\Psi^2(\theta)\Phi^2(\varphi) + \frac{\kappa}{\sin(\varphi)}\Psi^2(\theta)\left[\sin^2(\varphi)\left(\frac{\partial\Phi(\varphi)}{\partial\varphi}\right)^2 + \Phi^2(\varphi)\right] \right.$$
$$K_w R^2 \sin(\varphi)\,\Psi^2(\theta)\Phi^2(\varphi) + K_g\left[\sin(\varphi)\,\Psi^2(\theta)\left(\frac{\partial\Phi(\varphi)}{\partial\varphi}\right)^2 + \frac{1}{\sin(\varphi)}\left(\frac{\partial\Psi(\theta)}{\partial\theta}\right)^2\Phi^2(\varphi)\right]\Bigg\} d\varphi d\theta$$

$$K_{34} = \int_0^{\theta_1}\int_{\varphi_1}^{\varphi_2} \left\{ \kappa R A_{66}\sin(\varphi)\,\Psi^2(\theta)\left(\frac{\partial\Phi(\varphi)}{\partial\varphi}\right)^2 + \sin(\varphi) B_{12}\Psi^2(\theta)\frac{\partial^2\Phi(\varphi)}{\partial\varphi^2}\Phi(\varphi)\right.$$
$$+2B_{11}\cos(\varphi)\,\Psi^2(\theta)\frac{\partial\Phi(\varphi)}{\partial\varphi}\Phi(\varphi),$$

$$K_{35} = \int_0^{\theta_1}\int_{\varphi_1}^{\varphi_2} \left\{ \kappa R A_{66}\left(\frac{\partial\Psi(\theta)}{\partial\theta}\right)^2\Phi^2(\varphi) + B_{11}\frac{\partial^2\Psi(\theta)}{\partial\theta^2}\Psi(\theta)\Phi^2(\varphi)\right\} d\varphi d\theta,$$

$$K_{41} = K_{14}, \qquad K_{42} = K_{24}, \qquad K_{43} = K_{34},$$

$$K_{44} = \int_0^{\theta_1}\int_{\varphi_1}^{\varphi_2} \left\{ \kappa R^2 A_{66}\sin(\varphi)\,\Psi^2(\theta)\left(\frac{\partial\Phi(\varphi)}{\partial\varphi}\right)^2 + 2D_{12}\cos(\varphi)\Psi^2(\theta)\frac{\partial\Phi(\varphi)}{\partial\varphi}\frac{\partial^2\Phi(\varphi)}{\partial\varphi^2}\right.$$
$$+D_{11}\Psi^2(\theta)\left[\left(\frac{\partial^2\Phi(\varphi)}{\partial\varphi^2}\right)^2\sin(\varphi) + \left(\frac{\cos^2(\varphi)}{\sin(\varphi)}\right)\left(\frac{\partial\Phi(\varphi)}{\partial\varphi}\right)^2\right] + \frac{D_{66}}{\sin(\varphi)}\left(\frac{\partial\Psi(\theta)}{\partial\theta}\right)^2\left(\frac{\partial\Phi(\varphi)}{\partial\varphi}\right)^2\Bigg\} d\varphi d\theta,$$

$$K_{45} = \int_0^{\theta_1}\int_{\varphi_1}^{\varphi_2} \left\{ D_{11}\cot(\varphi)\,\Psi(\theta)\frac{\partial^2\Psi(\theta)}{\partial\theta^2}\frac{\partial\Phi(\varphi)}{\partial\varphi}\Phi(\varphi) + D_{12}\Psi(\theta)\frac{\partial\Psi^2(\theta)}{\partial\theta^2}\frac{\partial^2\Phi(\varphi)}{\partial\varphi^2}\Phi(\varphi)\right.$$
$$-D_{66}\frac{\partial\Psi^2(\theta)}{\partial\theta^2}\Psi(\theta)\frac{\partial^2\Phi(\varphi)}{\partial\varphi^2}\Phi(\varphi),$$

$$K_{51} = K_{15}, \qquad K_{52} = K_{25}, \qquad K_{53} = K_{35}, \qquad K_{55} = K_{45}$$

$$K_{55} = \int_0^{\theta_1}\int_{\varphi_1}^{\varphi_2} \left\{ \kappa R^2 A_{66}\sin(\varphi)\left(\frac{\partial\Phi(\varphi)}{\partial\varphi}\right)^2\Phi^2(\varphi) + \frac{D_{11}}{\sin(\varphi)}\left(\frac{\partial\Psi^2(\theta)}{\partial\theta^2}\right)^2\Phi^2(\varphi)\right.$$
$$+\left(\frac{\partial\Psi(\theta)}{\partial\theta}\right)^2\left[\left(\frac{\partial\Phi(\varphi)}{\partial\varphi}\right)^2\sin(\varphi) + \left(\frac{\cos^2(\varphi)}{\sin(\varphi)}\right)\Phi^2(\varphi) - 2\cos(\varphi)\,\Phi(\varphi)\frac{\partial\Phi(\varphi)}{\partial\varphi}\right]\Bigg\} d\varphi d\theta$$

- **Non-zero elements of Mass matrix**

$$M_{11} = \int_0^{\theta_1}\int_{\varphi_1}^{\varphi_2} J_0\Psi^2(\theta)\left(\frac{\partial\Phi(\varphi)}{\partial\varphi}\right)^2 R^2\sin(\varphi) d\varphi d\theta,$$

$$M_{14} = \frac{1}{2}\int_0^{\theta_1}\int_{\varphi_1}^{\varphi_2} J_1\Psi^2(\theta)\left(\frac{\partial\Phi(\varphi)}{\partial\varphi}\right)^2 R^2\sin(\varphi) d\varphi d\theta$$

$$M_{22} = \int_0^{\theta_1}\int_{\varphi_1}^{\varphi_2} J_0\left(\frac{\partial\Psi(\theta)}{\partial\theta}\right)^2\Phi^2(\varphi) R^2\sin(\varphi) d\varphi d\theta,$$

$$M_{25} = \frac{1}{2}\int_0^{\theta_1}\int_{\varphi_1}^{\varphi_2} J_0\left(\frac{\partial\Psi(\theta)}{\partial\theta}\right)^2\Phi^2(\varphi) R^2\sin(\varphi) d\varphi d\theta,$$

$$M_{33} = \int_0^{\theta_1}\int_{\varphi_1}^{\varphi_2} J_0\Psi^2(\theta)\Phi^2(\varphi) R^2\sin(\varphi) d\varphi d\theta,$$

$$M_{41} = M_{14},$$

$$M_{44} = \int_0^{\theta_1}\int_{\varphi_1}^{\varphi_2} J_2\Psi^2(\theta)\left(\frac{\partial\Phi(\varphi)}{\partial\varphi}\right)^2 R^2\sin(\varphi) d\varphi d\theta,$$

$$M_{52} = M_{25},$$

$$M_{55} = \int_0^{\theta_1}\int_{\varphi_1}^{\varphi_2} J_2\left(\frac{\partial\Psi(\theta)}{\partial\theta}\right)^2\Phi^2(\varphi) R^2\sin(\varphi) d\varphi d\theta,$$

- Non-zero elements of geometrical stiffness matrix

$$K_{g_{33}} = \int_{0}^{\theta_1} \int_{\varphi_1}^{\varphi_2} \left[N_{\varphi\varphi}^{0} \Psi^2(\theta) \left(\frac{\partial \Phi(\varphi)}{\partial \varphi} \right)^2 + \frac{N_{\theta\theta}^{0}}{\sin^2(\varphi)} \left(\frac{\partial \Psi(\theta)}{\partial \theta} \right)^2 \Phi^2(\varphi) + \frac{N_{\varphi\theta}^{0}}{\sin(\varphi)} \Psi(\theta) \frac{\partial \Psi(\theta)}{\partial \theta} \frac{\partial \Phi(\varphi)}{\partial \varphi} \Phi(\varphi) \right] \sin(\varphi)\, d\varphi d\theta$$